Research Article BEU Fen Bilimleri Dergisi 15(1): 350-359 (2026) DOI: 10.17798/bitlisfen.1810438

BİTLİS EREN UNIVERSITY
FEN BİLİMLERİ DERGİSİ
ISSN: 2147-3129 / e-ISSN: 2147-3188

INVESTIGATION OF THE HIGH TEMPERATURE RESISTANCE OF FOAM CONCRETE PRODUCED WITH DIFFERENT CEM-II TYPE CEMENTS

Selçuk MEMİŞ [1*], Hasbi YAPRAK [1], Emre KIVANÇ [2]

[1] *Kastamonu University, Department of Civil Engineering, Kastamonu, Türkiye*
[2] *Kastamonu University, Institute of Science, Department of Civil Engineering, Kastamonu, Türkiye*
**** Corresponding Author:*** *smemis@kastamonu.edu.tr*

Article Info

Received: *October 25, 2025*
Revised: *December 15, 2025*
Accepted: *January 17, 2026*

Keywords
Foam concrete,
CEM II/A-S,
CEM II/A-LL,
High temperature,
Water absorption rate,
Porosity,
UPV.

ABSTRACT

In this study, three foam concrete mixtures—each utilizing pumice aggregate and fixed foam/water content (240–50–220 g/dm³) but differing in binder type (PKB-1: CEM II/A-M (S–L); PKB-2: CEM II/A-S; PKB-3: CEM II/A-LL)—were comprehensively examined in terms of their fresh and hardened properties, permeability indicators, and high-temperature behavior. The mixtures were produced with constant mix ratios, and parameters such as density (fresh/hardened), total water absorption, open porosity, ultrasonic pulse velocity (UPV), and compressive strength at 3, 7, and 28 days were determined. For high-temperature evaluation, the specimens were exposed to 200, 400, 600, and 800 °C, and the corresponding mass loss and strength variation (%) were calculated. The results indicated that early-age mechanical development was strongly influenced by binder chemistry, with strength ranking at day 3 following the order PKB-2 > PKB-3 > PKB-1; by day 7, these differences had narrowed, and by 28-day, all three systems converged to approximately 10.5–10.8 MPa. Although PKB-2 exhibited the highest unit weight, it also demonstrated the greatest porosity and water absorption. Ultrasonic pulse velocity showed a positive correlation with density and a negative correlation with porosity within the same density range. As temperature increased, mass loss gradually rose, converging at around 18–20% at 800 °C. Limited strength gains were observed between 200 °C and 400 °C due to internal water redistribution and gel relaxation, while all mixtures exhibited significant strength reductions at ≥600 °C; the limestone-based system (PKB-3) showed more pronounced losses associated with $CaCO_3$ decomposition. Overall, CEM II/A-LL proved suitable for lightweight elements requiring low water absorption, CEM II/A-S for applications prioritizing early-age strength, and CEM II/A-M (S–L) provided a balanced design window between mechanical, transport, and thermal stability.

1. INTRODUCTION

Foam concrete—also known as cellular concrete or aerated concrete—is a cementitious composite produced by introducing air voids into a fresh mortar mixture in a controlled manner using foaming agents. This technique generates a trapped, porous microstructure that imparts significantly lower density and superior thermal insulation properties compared to conventional concrete. [1–3]. The porous cellular structure uniformly distributed throughout the hardened concrete ensures continuity in thermal and acoustic performance and, when adequately stabilized, also enhances the material's workability [2,3].

An examination of the historical development of cementitious materials containing foam reveals that the concept was largely shaped around autoclaved aerated concrete (AAC). Commercial products such as Ytong, first produced in the 1920s, represent the pioneering applications of this material. Following these early advancements, the introduction of chemical agents developed by the construction-related chemical industry led to the emergence of foam concretes, which have since been associated with aerated

concrete technologies. The development of foam concretes with varying densities, binder compositions, and admixture systems has been extensively studied in the literature, with numerous investigations focusing on their durability and performance relationships [1,3]

The most distinctive advantage of foam concrete is its low dry density. This property reduces the dead load of structures, allowing for longer spans or lighter load-bearing systems, while also limiting heat transfer through building envelopes, thereby enhancing the overall energy efficiency of the structure [2–4]. The density of the material can be controlled by adjusting the foam volume, the properties of the foaming agent, and the compaction methods used during the mixing process. As a result, foam concrete is typically produced within a wide density range, from a few hundred kilograms per cubic meter up to approximately 1000 kg/m³ [3,4]. The size distribution, spacing, and morphology of air voids directly influence the thermal resistance, mechanical behavior, and moisture transport characteristics of the hardened concrete. A homogeneous and well-dispersed pore structure ensures stable performance, whereas irregular or clustered voids can lead to localized stress concentrations and increased permeability issues [2,3]. Therefore, in foam concretes, the balance between lightness and structural integrity largely depends on the microstructure of the air voids [3].

From a sustainability perspective, foam concretes are gaining increasing importance in modern construction. Their low density allows for reduced binder consumption per unit volume, while their high thermal resistance decreases heating and cooling loads in wall and roof elements, thereby reducing overall energy consumption [4,5]. Thanks to their thermal insulation properties, foam concretes provide lower heat flux and, consequently, greater occupant comfort—offering a valuable contribution to meeting energy standards and achieving sustainable building certifications [5,6]. Considering the environmental impacts of cementitious materials, the use of alternative binders, pozzolanic additives, and low-emission cements (including CEM II variants) has been shown to significantly influence both the mechanical and durability properties of foam concrete [4,7,8]. Studies on concrete sustainability have demonstrated that the partial replacement of Portland cement with industrial by-products or fly ash–blended cements reduces the adverse impacts observed throughout the material's life cycle while maintaining an acceptable level of performance [4,8,9]. This becomes even more significant for foam concrete, in which the binder content plays a critical role in determining both density and thermal behavior [4,5,9].

High-temperature resistance and fire safety are critical attributes for modern construction materials in terms of structural integrity. Under fire or extreme heat conditions, concrete elements are expected to maintain their load-bearing capacity long enough to allow safe evacuation, reduce the risk of collapse, and provide thermal protection for embedded components [10–12]. The literature indicates that elevated temperatures reduce the compressive strength of cementitious materials, with the extent of this reduction depending on factors such as binder type, aggregate characteristics, porosity, and the applied cooling regime [10], [11]Studies have revealed that the type of cement and the incorporated additives influence heat transfer, pore structure stability, and damage mechanisms under elevated temperature conditions [11,12]. In the case of foam concrete, the interaction between the air-void microstructure and exposure to high temperatures makes the degradation mechanisms more complex, highlighting the need for specific data on CEM II–based foam concretes. [1,2,10].

Although foam concretes are widely used in energy-efficient construction, systematic studies focusing on those produced with CEM II-type cements remain limited. While the existing literature addresses various binder and admixture systems, there is still a lack of comprehensive research on the high-temperature performance, long-term durability, and pore structure–thermal damage interactions of CEM II–based foam concretes [1,4,7]. Recent studies have focused on the durability of low-emission or blended cements; however, these investigations do not directly examine the unique microstructure of foam concrete under fire-like conditions [7,8,10]. Therefore, there remains a need for quantitative data on CEM II–based foam concretes under high-temperature conditions, particularly regarding compressive strength, density variations, and the evolution of the air-void structure [1–3]. This study aims to address this research gap by providing experimental data on the high-temperature resistance of foam concretes produced with CEM II-type cements, thereby generating new evidence at the intersection of fire safety and sustainability.

The objectives of this study can be summarized under three main headings: (i) to characterize the fresh-state behavior, microstructure, and density of foam concretes produced with CEM II-type cements; (ii) to evaluate their mechanical performance both under ambient conditions and after exposure to elevated temperatures; and (iii) to compare the high-temperature behavior of different CEM II variants and foam systems in order to identify the key parameters governing thermal resistance and to assess the potential for post-cooling performance recovery. By considering the decisive effects of density and porosity on thermal and mechanical responses, this study—focused on CEM II binder systems—aims to provide new insights for the development of sustainable and fire-resistant construction materials [3,4,7,8]. The compressive strength, density, and microstructural data obtained from this study will demonstrate the potential of CEM II–based foam concretes for energy-efficient, low-emission, and fire-safe applications, while also providing a foundation for future research on their long-term durability [1,2,10,11].

2. MATERIALS AND METHOD

In all mixtures used in this study (Figure 1), the aggregate, cement, foam, and water contents were kept constant, with only the type of cement being varied. Fine pumice from Nevşehir, passing through a 2 mm sieve, was employed as the lightweight aggregate, selected for its high open porosity and low particle density [13,14]. Three types of cement conforming to EN 197-1 were used as binders: Portland Composite Cement (CEM II/A-M (S–L)), Portland Slag Cement (CEM II/B-S), and Portland Limestone Cement (CEM II/A-LL). The mixing water met the requirements of EN 1008. In the design of the mixtures in this study, the target unit weight was determined to be within the lightweight mortar class, taking into account the unit volume mass of the pumice aggregate used and a fixed foam dosage (50 g/dm³). Within this scope, the target fresh unit weight for the samples was selected to be in the range of approximately 0.90–1.20 g/cm³ (900–1200 kg/m³). In accordance with the widely adopted preformed foam method reported in the literature, a stable foam was produced using a commercial preformed foaming agent [15] supplied by Fatsa Kimya ve Tic. Ltd. Şti. The specific properties of the cements used in the mixtures are presented in Table 1, while the chemical composition of the pumice is given in Table 2.

(a) **(b)**

Figure 1. Using materials a*) pumice, b) foam*

Table 1. Cement types used in mixtures and some of their properties

		CEM II/A-M (S-L) (Portland Composite Cement)	**CEM II / A – S (Portland Slag Cement)**	**CEM II / A – LL (Portland Limestone Cement)**
Clinker		80-88 %	65-79 %	80-94
		12-20 % Limestone+Slag	0-5 % Limestone	6-20 % Limestone
Setting regulator		Calcium sulfate	Calcium sulfate	Calcium sulfate
SO_3		<4 %	(2,73) <4 %	<4 %
Cl		<0,10 %	<0,10 %	<0,10 %
Setting start (min)		>60 min	>60 min (201 min)	>60 min
Volume expansion (mm)		<10	<10	<10
Compressive strength (MPa)	2nd day	20	24,7	20
	28nd day	42,5	47,9	42,5

Table 2. XRF result of pumice aggregate

Oxide	SiO_2	Al_2O_3	Fe_2O_3	CaO	MgO	SO_3	K_2O	Na_2O
Pumice	73.78	12.19	3.266	2.611	0.736	0.0491	2.387	2.443

Three different mixtures with a water-to-binder ratio of 0.55 were produced using identical volumetric components (determined through preliminary trials), and the "foam content" was kept constant across all groups. In the foam mixtures (Figure 2), the foam was prepared using a chemical foaming method. For foam generation, 10 g of foaming agent was dissolved in 100 mL of water, producing foam with a density of 98 g/L, which was subsequently incorporated into the mixtures. This method was chosen to achieve a homogeneous pore distribution and a low-density structure. The detailed mix design is presented in Table 3.

Table 3. Mix design

Group	Pumice (g/dm^3)	Cement type	Cement (g/dm^3)	Foam (g/dm^3)	Water (g/dm^3)
PKB-1	240	CEM II/A-M (S-L)	400	50	220
PKB-2	240	CEM II / A – S	400	50	220
PKB-3	240	CEM II / A - LL	400	50	220

The dry components (cement and pumice) were first mixed at low speed for 2 minutes to ensure homogeneity, after which the mixing water was added, and the mixture was homogenized for an additional 5 minutes. The preformed foam—prepared according to the manufacturer's target foam density—was then slowly incorporated into the mix at a low rotation speed to minimize bubble coalescence, following the procedures recommended for foamed concretes[15]. The fresh mixtures were cast into 40×40×160 mm prismatic molds, the surfaces were leveled, and the molds were covered with polyethylene film and kept in an oven at (45 ± 2 °C) for 24 hours.

PKB-1 **PKB-2** **PKB-3**

Figure 2. Foam samples produced and used in mixtures

Subsequently, the samples (Figure 2) were cured at 60 °C and 90% relative humidity for 48 hours and stored under laboratory conditions until the relevant experimental process. After curing, the samples were tested for water absorption, dry unit weight, and porosity in accordance with ASTM C642 [16], ultrasonic pulse velocity (UPV) according to TS EN 12504-4 [17], and flexural and compressive strength following TS EN 196-1[18]. Weight and strength losses at 200, 400, 600, and 800 °C were determined according to the procedures described in [19,20]. UPV measurements were performed using the surface transmission (transducer-to-transducer) method as specified in ASTM C597 [21]. The results were interpreted with respect to matrix continuity and sensitivity to compaction and porosity variations [13,22].

3. RESULTS AND DISCUSSION

In pumice-based foam concretes prepared with a constant foam ratio and water content—where only the binder type was varied—the unit weight (Figure 3) was found to be highest in the CEM II/A-S (PKB-2) group, followed by CEM II/A-LL (PKB-3), and lowest in CEM II/A-M (S–L) (PKB-1). Conversely,

in terms of porosity, the highest value was again observed in CEM II/A-S (PKB-2), followed by CEM II/A-LL (PKB-3), while the lowest was recorded for CEM II/A-M (S–L) (PKB-1). The water absorption results supported this trend, showing the highest value for CEM II/A-S, the lowest for CEM II/A-LL, and an intermediate value for CEM II/A-M (S–L). Accordingly, CEM II/A-S exhibited an exceptional behavior compared to the general trend widely reported in the foam concrete literature—where increased density typically corresponds to reduced porosity and water absorption—by presenting both higher density and elevated porosity/water absorption values simultaneously. This deviation indicates that permeability-related indicators in foam concrete are not governed solely by density, but are also strongly influenced by morphological factors such as bubble coalescence, pore size distribution, and connectivity, as well as by mixture rheology and foam stability [13–15,23].

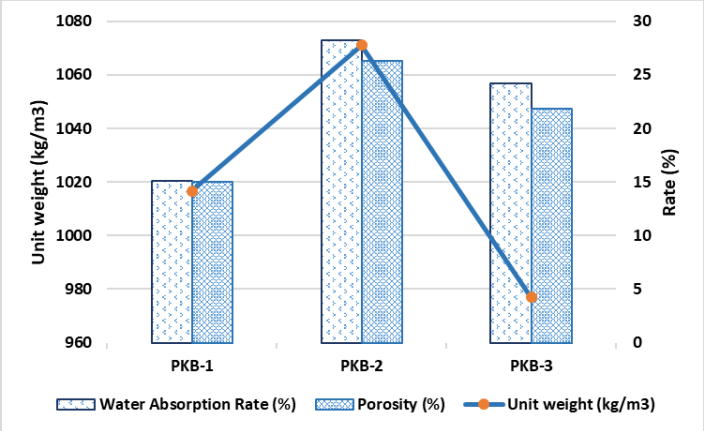

Figure 3. Changes in water absorption rate, unit volume weight and porosity of the mixtures

In slag-based binders (CEM II/A-S), the long-term formation of C-(A)-S-H gel has the potential to reduce transport properties by refining microcapillary pores; however, in the context of foam concrete, increasing slag content and foam volume can adversely affect viscosity and stability, promoting the development of larger and more interconnected pore networks. This, in turn, may lead to increased water absorption and porosity [24,25]. Conversely, limestone-blended cements (CEM II/A-LL) can accelerate the precipitation of early hydration products through the "filler/nucleation" effect, resulting in a denser and finer-pored matrix. Although this generally lowers water absorption, the extent of the effect depends on particle size and dosage [26,27]. The hybrid system (CEM II/A-M (S–L)), combining slag and limestone, benefits from enhanced particle packing and a Ca-enriched gel structure, which together tend to yield lower permeability. Nevertheless, in foam concretes, the porous nature of pumice and the characteristics of the interfacial transition zone (ITZ) significantly influence total porosity, water absorption, and the density–porosity relationship [13]. Overall, when examining the variations observed in this study, the high density accompanied by elevated porosity and water absorption in CEM II/A-S (PKB-2), the low water absorption in CEM II/A-LL (PKB-3), and the relatively balanced permeability in CEM II/A-M (S–L) (PKB-1) are consistent with microstructure- and rheology-based interpretations reported in previous foam concrete studies.

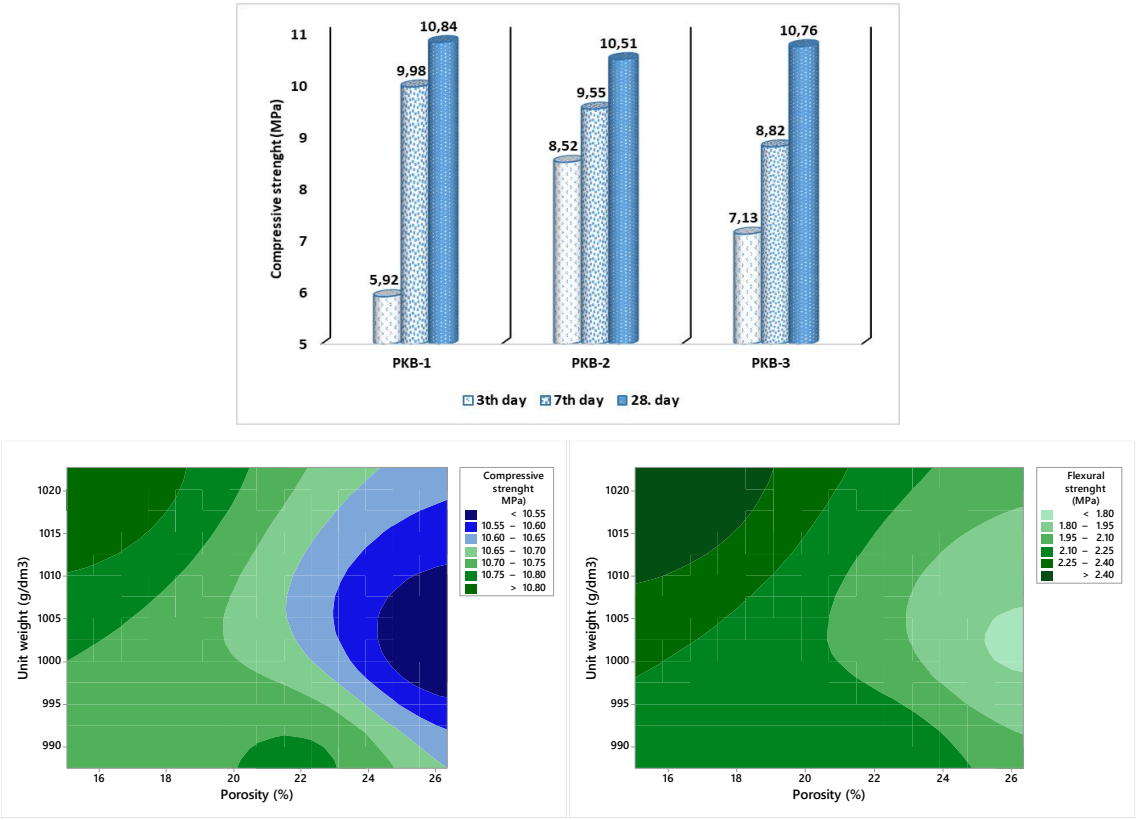

Figure 4. Change between compressive and flexural strength values and porosity/unit weight

When the compressive strengths of foam concrete mixtures with varying binder types were examined (Figure 4), the results showed that for the PKB-1 (CEM II/A-M (S–L)), PKB-2 (CEM II/A-S), and PKB-3 (CEM II/A-LL) groups, the strength ranking at 3 days followed the order PKB-2 > PKB-3 > PKB-1. By day 7, the values had converged, and by day 28, all series reached approximately 10.5–10.8 MPa, with PKB-1 achieving the highest final strength. These findings clearly demonstrate the relationship between binder composition, microstructure and the interdependence of mechanical and transport properties. The role of binder type supports this pattern: in slag-based systems (CEM II/A-S), long-term C-(A)-S-H gel formation has the potential to fill microcapillary pores and reduce transport properties. However, in foam concrete, the interaction between slag content, paste viscosity, and foam stability can promote the formation of large, interconnected pore networks, leading to higher water absorption and porosity; the coexistence of high density and high permeability in PKB-2 reflects this mechanism [24,25]. In limestone-blended cement (CEM II/A-LL), the “filler/nucleation” effect accelerates early hydration, producing a denser and finer pore structure, thereby reducing water absorption, although the magnitude of this effect depends on particle size and dosage Additionally, the open porosity of pumice and the characteristics of the interfacial transition zone (ITZ), together with matrix architecture, play a decisive role in governing total porosity and water absorption.

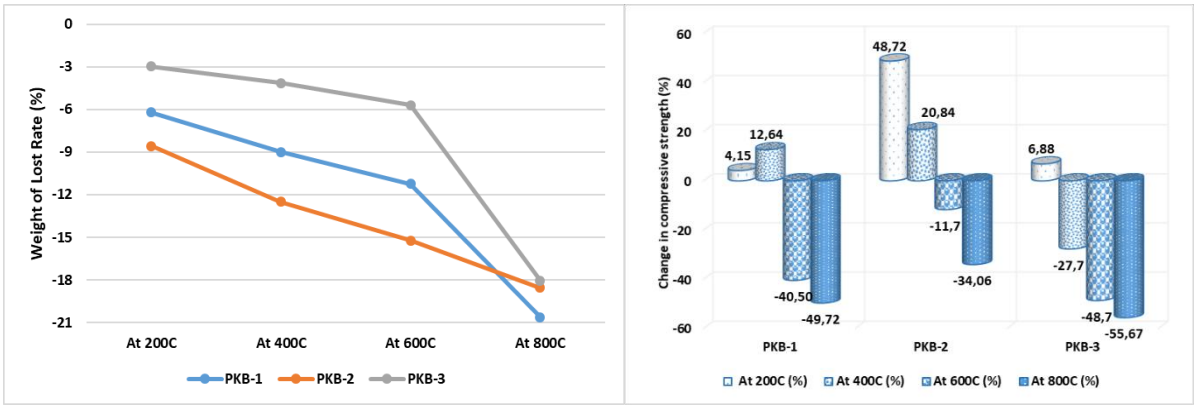

Figure 5. Change in weight and strength after high temperature

When the high-temperature and non-destructive evaluation results of the PKB-1 (CEM II/A- M (S–L)), PKB-2 (CEM II/A-S), and PKB-3 (CEM II/A-LL) groups were examined (Figure 5), a consistent overall pattern was observed. As temperature increased within the 200–800 °C range, mass loss gradually rose across all mixtures, converging at approximately 18–20% at 800 °C. Among these, the lowest mass loss between 200 °C and 600 °C was recorded in PKB-3, which was produced with the limestone-based binder. Regarding compressive strength variations, PKB-1 (S–L) exhibited a moderate increase between 200 °C and 400 °C followed by a marked decrease from 600 °C to 800 °C. PKB-2 (slag-based) showed a more pronounced strength gain between 200 °C and 400 °C before declining at higher temperatures (600–800 °C). In contrast, PKB-3 (limestone-based) displayed a slight increase at 200 °C, followed by a continuous reduction from 400 °C to 800 °C.

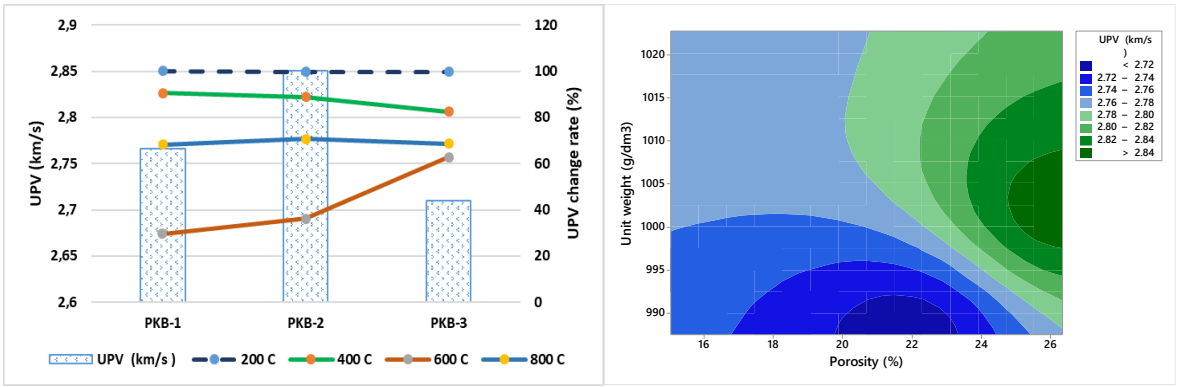

Figure 6. Changes between UPV values and porosity/unit volume weight before/after high temperature

These results demonstrate that UPV is highly sensitive to matrix continuity and pore connectivity. The observed pattern aligns well with findings in the literature, which report that limited strength gains occurring at 200–300 °C are primarily due to internal water redistribution and gel-phase relaxation, whereas significant strength losses beyond 400–600 °C are attributed to the evaporation of free and chemically bound water, $Ca(OH)_2$ decomposition, alterations in gel morphology, and microcracking. In slag-based systems, long-term filling of microcapillaries by C-(A)-S-H gel is expected; however, in the case of foam concrete, the interaction among rheology, foam stability, and curing conditions can promote the formation of large, interconnected pore networks, thereby increasing water absorption and porosity. The strength gains of PKB-2 between 200 °C and 400 °C, along with its high permeability indicators, can be explained by this mechanism [23]. In limestone-blended systems, the "filler/nucleation" effect enhances early-age particle packing and reduces water absorption, although this effect is sensitive to dosage and fineness. Moreover, at 700–800 °C, $CaCO_3$ decomposition accelerates microcracking and strength loss, which is consistent with the behavior observed in PKB-3 [26]. Ultimately, it was concluded that density alone is not a sufficient indicator of performance; the primary variables governing permeability are pore size distribution and connectivity. Therefore, UPV and compressive strength

should be interpreted in conjunction with the rheology-based pore architecture of the material [13–15,22].

The bubble chart (Figure 7) (where the x-axis represents porosity (%), the y-axis represents unit weight (g/dm³), and bubble area corresponds to UPV (km/s)) illustrates the relationship between void architecture, density, and matrix continuity across the three mixtures. PKB-2 (CEM II/A-S) is positioned in the high-porosity (~26–27%) and medium-to-high-density (~1005 g/dm³) region, exhibiting the lowest UPV, which suggests a well-developed network of interconnected voids within the matrix. PKB-1 (CEM II/A-M (S–L)), on the other hand, shows very low porosity (~16%) and the highest density (~1023–1025 g/dm³) accompanied by a high UPV value, indicating a continuous, compact matrix with limited connectivity. Interestingly, PKB-3 (CEM II/A-LL) demonstrates a lower density (~998–1000 g/dm³) and moderate porosity (~21–22%), yet displays a large bubble size corresponding to high UPV. This behavior is consistent with the "filler/nucleation" effect of limestone, which promotes a finer and more closed pore structure, facilitating ultrasonic wave propagation. Overall, the chart reveals that UPV is sensitive not only to density but also to pore size distribution and connectivity. The dominant mechanisms appear to be coalescence and large/interconnected void formation in the slag-based system (PKB-2) and pore refinement in the limestone-based system (PKB-3). These interpretations align with literature emphasizing the interdependence of UPV, density, and porosity, as well as the influence of binder type on pore morphology in foam concretes [13,14,22,26,28].

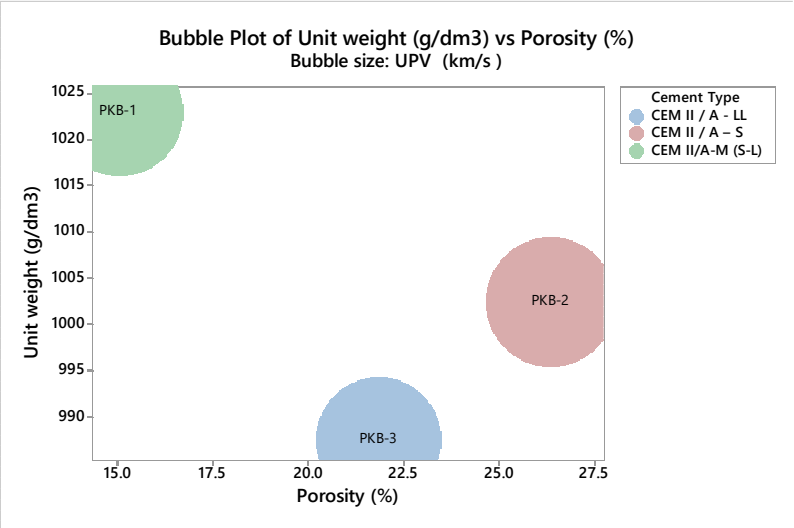

Figure 7. UPV distribution according to cement type in unit weight/porosity matrix

4. CONCLUSION AND SUGGESTIONS

This study evaluated the influence of binder type on the fresh, mechanical, transport, and high-temperature performance of pumice-based foam concretes produced with constant foam and water contents. The results demonstrate that binder mineralogy plays a critical role in governing pore structure and its continuity, which in turn controls density, water absorption, mechanical behavior, and thermal stability. While all mixtures achieved comparable 28-day compressive strengths in the range of 10.5–10.8 MPa, differences in early-age performance and durability-related properties were evident. The slag-based binder enhanced early strength and density but was associated with increased interconnected porosity and water absorption when foam stability was insufficient. In contrast, the limestone-based binder resulted in lower water absorption and a more stable pore system at ambient conditions, although it exhibited greater strength loss at 800 °C due to $CaCO_3$ decomposition. The hybrid S–L binder provided the most balanced overall performance, showing stable mechanical behavior, moderate transport properties, and improved thermal resistance across the investigated temperature range. These findings highlight that effective foam stability and pore connectivity control are as important as binder selection in the design of foam concretes. Within the limitations of the present study, the hybrid binder system appears to offer a promising design window for lightweight structural and non-structural applications requiring a balanced combination of strength, durability, and high-temperature resistance.

Overall, the limestone-based binder appears suitable for lightweight applications requiring low water absorption, while the slag-based binder offers advantages in early strength development. However, excessive interconnected porosity in slag-rich systems may compromise transport resistance if foam stability is not adequately controlled. The hybrid S–L binder provides a balanced compromise between mechanical performance, durability, and thermal stability. Improvements in slag-based systems may be achieved through enhanced rheological control and foam stabilization, whereas limestone-based systems require careful adjustment of fineness and dosage to maintain thermal resistance.

Considering the limitations of this study—namely constant foam and water contents, a single aggregate type, and a limited binder selection—future research should focus on detailed pore structure analysis (e.g., MIP or μ-CT), ITZ characterization (SEM–EDS), and correlations between residual mechanical properties and UPV after thermal exposure.

Conflict of Interest Statement

There is no conflict of interest between the authors.

Statement of Research and Publication Ethics

The study is complied with research and publication ethics.

Artificial Intelligence (AI) Contribution Statement

In this study, artificial intelligence (AI) tools were used solely for purpose of improving the grammatical accuracy and linguistic clarity of the English text. All scientific content, including data analysis, figures, and the manuscript's structural composition, was entirely generated by the authors without any AI assistance.

Contributions of the Authors

S.M. and H.Y. designed the study, S.M., H.Y., and E.K. performed the experiments, and S.M. and E.K. wrote the paper. S.M. and H.Y. performed the calculations, checked the language, and contributed to the writing of the paper.

REFERENCES

[1] G. Zhou, R.K. Leung Su, A review on serviceability of foam concrete, Proc. Inst. Civ. Eng. Constr. Mater. 177 (2024) 381–392. https://doi.org/10.1680/jcoma.24.00004.

[2] M. Davraz, S. Kilinçarslan, M. Koru, F. Tuzlak, Investigation of relationships between ultrasonic pulse velocity and thermal conductivity coefficient in foam concretes, Acta Phys. Pol. A. 130 (2016) 469–470. https://doi.org/10.12693/APhysPolA.130.469.

[3] E. Ikponmwosa, F. Falade, C. Fapohunda, A review and investigations of some properties of foamed aerated concrete, Niger. J. Technol. 33 (2014) 1. https://doi.org/10.4314/njt.v33i1.1.

[4] A. Król, Z. Giergiczny, J. Kuterasinska-Warwas, Properties_of_concrete_made_with_recycle, Materials (Basel). (2019) 2257.

[5] K.T. Wan, H. Zhu, T.Y.P. Yuen, B. Chen, C. Hu, C.K.Y. Leung, J.S. Kuang, Development of low drying shrinkage foamed concrete and hygro-mechanical finite element model for prefabricated building fasçade applications, Constr. Build. Mater. 165 (2018) 939–957. https://doi.org/10.1016/j.conbuildmat.2018.01.024.

[6] S.J. Yu, Y.L. Wang, B.J. Duan, J.W. Zhou, F. Yang, X.G. Wang, D.L. Liang, Fireproof Performance of Foam Concrete Insulation Board, Adv. Mater. Res. 250–253 (2011) 474–479. https://doi.org/10.4028/www.scientific.net/AMR.250-253.474.

[7] L. Húlek, M. Ba, M. Cápay, I. Janotka, Perspective of concrete with portland composite cement CEM II/C-M (S-LL), 29 (2024) 54–70.

[8] K. Křížová, P. Novosad, T. Jarolím, Production of Self Compacting Concrete SCC with Portland and Blended Cement CEM I, CEM II with Fly Ash and Limestone Admixtures, Adv. Mater. Res. 1124 (2015) 45–50. https://doi.org/10.4028/www.scientific.net/AMR.1124.45.

[9] M.W. Tait, W.M. Cheung, A comparative cradle-to-gate life cycle assessment of three concrete mix designs, Int. J. Life Cycle Assess. 21 (2016) 847–860. https://doi.org/10.1007/s11367-016-1045-5.

[10] E. Klingsch, A. Frangi, M. Fontana, Experimental Analysis of Concrete Strength at High Temperatures

and after Cooling, Acta Polytech. 49 (2009). https://doi.org/10.14311/1087.

[11] T. McKenna, M.G. Richardson, B. O'Rourke, Heat Transfer Characteristics of GGBS Concrete in Fire, J. Sustain. Archit. Civ. Eng. 8 (2014) 45–58. https://doi.org/10.5755/j01.sace.8.3.7457.

[12] P. Kirton, A. Richardson, B. Agnew, Thermo-mechanical performance of concrete with alternative binder material, Struct. Surv. 31 (2013) 368–386. https://doi.org/10.1108/SS-01-2013-0002.

[13] O. Gencel, T. Bilir, Z. Bademler, T. Ozbakkaloglu, A Detailed Review on Foam Concrete Composites: Ingredients, Properties, and Microstructure, Appl. Sci. 12 (2022). https://doi.org/10.3390/app12115752.

[14] E.P. Kearsley, P.J. Wainwright, Porosity and permeability of foamed concrete, Cem. Concr. Res. 31 (2001) 805–812. https://doi.org/10.1016/S0008-8846(01)00490-2.

[15] E.K.K. Nambiar, K. Ramamurthy, Sorption characteristics of foam concrete, Cem. Concr. Res. 37 (2007) 1341–1347. https://doi.org/10.1016/j.cemconres.2007.05.010.

[16] ASTM C642-21. Standard Test Method for Density, Absorption, and Voids in Hardened Concrete, n.d.

[17] TS EN 12504-4. Testing concrete in structures - Part 4: Determination of ultrasonic pulse velocity, n.d.

[18] TS EN 196-1. Methods of testing cement - Part 1: Determination of strength, 2016.

[19] A. Moosavi, S. Asadi, H.J. Shoraki, Microstructure and mechanical properties of tabular alumina composites with geopolymer binder at elevated temperatures, Ceram. Int. 45 (2019) 9092–9098. https://doi.org/10.1016/j.ceramint.2019.01.246.

[20] Z. Zhang, J.L. Provis, A. Reid, H. Wang, Mechanical, thermal insulation, thermal resistance and acoustic absorption properties of geopolymer foam concrete, Cem. Concr. Compos. 62 (2015) 97–105. https://doi.org/10.1016/j.cemconcomp.2015.03.013.

[21] ASTM 597 - 22 Standard Test Method for Pulse Velocity Through Concrete, n.d.

[22] C. Liu, G. Liu, Characterization of pore structure parameters of foam concrete by 3D reconstruction and image analysis, Constr. Build. Mater. 267 (2021) 120958. https://doi.org/10.1016/j.conbuildmat.2020.120958.

[23] A. Jierula, H. Li, Y. Chen, C. Wu, X. Wu, H. Yin, Study on the Influence of Density and Water–Cement Ratio on the Cement Utilization, Fluidity, Mechanical Properties, and Water Absorption of Foam Concrete, Buildings. 14 (2024) 1–17. https://doi.org/10.3390/buildings14113550.

[24] O.H. Oren, A. Gholampour, O. Gencel, T. Ozbakkaloglu, Physical and mechanical properties of foam concretes containing granulated blast furnace slag as fine aggregate, Constr. Build. Mater. 238 (2020) 117774. https://doi.org/10.1016/j.conbuildmat.2019.117774.

[25] S.K. Jose, M. Soman, Y. Sheela Evangeline, Ecofriendly building blocks using foamed concrete with ground granulated blast furnace slag, Int. J. Sustain. Eng. 14 (2021) 776–784. https://doi.org/10.1080/19397038.2020.1836064.

[26] A.A. Elgalhud, R.K. Dhir, G. Ghataora, Limestone addition effects on concrete porosity, Cem. Concr. Compos. 72 (2016) 222–234. https://doi.org/10.1016/j.cemconcomp.2016.06.006.

[27] G. Li, H. Tan, X. He, J. Zhang, X. Deng, Z. Zheng, Research on the properties of wet-ground waste limestone powder as foam stabilizer in foamed concrete, Constr. Build. Mater. 329 (2022) 127203. https://doi.org/10.1016/j.conbuildmat.2022.127203.

[28] E.K.K. Nambiar, K. Ramamurthy, Models for strength prediction of foam concrete, Mater. Struct. Constr. 41 (2008) 247–254. https://doi.org/10.1617/s11527-007-9234-0.